Research Article | Vol. 26, No. 13 | 25 Jun 2018 | OPTICS EXPRESS 17360
Optics EXPRESS

Polarization-multiplexed nonlinear inverse synthesis with standard and reduced-complexity NFT processing

S. Civelli,[1,2,*] S. K. Turitsyn,[2] M. Secondini,[1] and J. E. Prilepsky[2]

[1]TeCIP Institute, Scuola Superiore Sant'Anna, Pisa, Italy
[2]Aston Institute of Photonic Technologies, Aston University, Birmingham, UK
[*]stella.civelli@santannapisa.it

Abstract: In this work, we study the performance of polarization division multiplexing nonlinear inverse synthesis transmission schemes for fiber-optic communications, expected to have reduced nonlinearity impact. Our technique exploits the integrability of the Manakov equation—the master model for dual-polarization signal propagation in a single mode fiber—and employs nonlinear Fourier transform (NFT) based signal processing. First, we generalize some algorithms for the NFT computation to the two- and multicomponent case. Then, we demonstrate that modulating information on both polarizations doubles the channel information rate with a negligible performance degradation. Moreover, we introduce a novel dual-polarization transmission scheme with reduced complexity which separately processes each polarization component and can also provide a performance improvement in some practical scenarios.

OCIS codes: (060.1660) Coherent communications; (060.2330) Fiber optics communications; (060.4370) Nonlinear optics, fibers.

References and links

1. D. J. Richardson, "Filling the light pipe," Science **330**, 327–328 (2010).
2. R.-J. Essiambre, G. Kramer, P. J. Winzer, G. J. Foschini, and B. Goebel, "Capacity limits of optical fiber networks," J. Lightw. Technol. **28**, 662–701 (2010).
3. J. C. Cartledge, F. P. Guiomar, F. R. Kschischang, G. Liga, and M. P. Yankov, "Digital signal processing for fiber nonlinearities," Opt. Express **25**, 1916–1936 (2017).
4. S. K. Turitsyn, J. E. Prilepsky, S. T. Le, S. Wahls, L. L. Frumin, M. Kamalian, and S. A. Derevyanko, "Nonlinear Fourier transform for optical data processing and transmission: advances and perspectives," Optica **4**, 307–322 (2017).
5. V. Zakharov and A. Shabat, "Exact theory of two-dimensional self-focusing and one-dimensional self-modulation of waves in nonlinear media," Sov. Phys. JETP **34**, 62 (1972).
6. M. J. Ablowitz and H. Segur, *Solitons and the Inverse Scattering Transform*, vol. 4 (SIAM, 1981).
7. M. J. Ablowitz, B. Prinari, and A. D. Trubatch, *Discrete and Continuous Nonlinear Schroedinger Systems* (Cambridge University, 2004).
8. A. Hasegawa and T. Nyu, "Eigenvalue communication," J. Lightw. Technol. **11**, 395–399 (1993).
9. M. I. Yousefi and F. R. Kschischang, "Information transmission using the nonlinear Fourier transform, Parts I–III," IEEE Trans. Inf. Theory **60**, 4312–4369 (2014).
10. S. V. Manakov, "On the theory of two-dimensional stationary self-focusing of electromagnetic waves," Sov. Phys. JETP **38**, 248–253 (1974).
11. M. I. Yousefi and X. Yangzhang, "Linear and nonlinear frequency-division multiplexing," European Conference on Optical Communication (ECOC 2016), Proceedings of (2016).
12. H. Bülow, "Experimental demonstration of optical signal detection using nonlinear Fourier transform," J. Lightw. Technol. **33**, 1433–1439 (2015).
13. V. Aref, S. T. Le, and H. Buelow, "Modulation over nonlinear Fourier spectrum: Continuous and discrete spectrum," J. Lightw. Technol. **36**, 1289–1295 (2018).
14. I. Tavakkolnia and M. Safari, "Capacity analysis of signaling on the continuous spectrum of nonlinear optical fibers," J. Lightw. Technol. **35**, 2086–2097 (2017).

#330332 https://doi.org/10.1364/OE.26.017360
Journal © 2018 Received 26 Apr 2018; revised 6 Jun 2018; accepted 7 Jun 2018; published 20 Jun 2018

Optics EXPRESS

15. S. T. Le, I. D. Philips, J. E. Prilepsky, P. Harper, A. D. Ellis, and S. K. Turitsyn, "Demonstration of nonlinear inverse synthesis transmission over transoceanic distances," J. Lightw. Technol. **34**, 2459–2466 (2016).
16. S. T. Le, V. Aref, and H. Buelow, "Nonlinear signal multiplexing for communication beyond the Kerr nonlinearity limit," Nat. Photon. **11**, 570 (2017).
17. M. Kamalian, J. E. Prilepsky, S. T. Le, and S. K. Turitsyn, "Periodic nonlinear Fourier transform for fiber-optic communication, part II: Eigenvalue communication," Opt. Express **24**, 18370–18381 (2016).
18. J. E. Prilepsky, S. A. Derevyanko, K. J. Blow, I. Gabitov, and S. K. Turitsyn, "Nonlinear inverse synthesis and eigenvalue division multiplexing in optical fiber channels," Phys. Rev. Lett. **113**, 013901 (2014).
19. C. R. Menyuk and B. S. Marks, "Interaction of polarization mode dispersion and nonlinearity in optical fiber transmission systems," J. Lightw. Technol. **24**, 2806 (2006).
20. A. Maruta and Y. Matsuda, "Polarization division multiplexed optical eigenvalue modulation," in "Photonics in Switching (PS), 2015 International Conference on," (IEEE, 2015), pp. 265–267.
21. J.-W. Goossens, M. I. Yousefi, Y. Jaouën, and H. Hafermann, "Polarization-division multiplexing based on the nonlinear Fourier transform," Opt. express **25**, 26437–26452 (2017).
22. S. Gaiarin, A. M. Perego, E. P. da Silva, F. Da Ros, and D. Zibar, "Dual-polarization nonlinear Fourier transform-based optical communication system," Optica **5**, 263–270 (2018).
23. S. Gaiarin, A. M. Perego, E. P. da Silva, F. Da Ros, and D. Zibar, "Experimental demonstration of dual polarization nonlinear frequency division multiplexed optical transmission system," in "43rd European Conference on Optical Communications (ECOC)," (2017), p. W.3.C.2.
24. N. A. Shevchenko, S. A. Derevyanko, J. E. Prilepsky, A. Alvarado, P. Bayvel, and S. K. Turitsyn, "Capacity lower bounds of the noncentral chi-channel with applications to soliton amplitude modulation," IEEE Trans. Commun. **66** (2018).
25. T. Gui, W. A. Gemechu, J.-W. Goossens, M. Song, S. Wabnitz, M. I. Yousefi, H. Hafermann, A. P. T. Lau, and Y. Jaouën, "Polarization-division-multiplexed nonlinear frequency division multiplexing," in "CLEO: Science and Innovations," (Optical Society of America, 2018), pp. STu4C–3.
26. S. Le, I. Philips, J. Prilepsky, M. Kamalian, A. Ellis, P. Harper, and S. Turitsyn, "Equalization-enhanced phase noise in nonlinear inverse synthesis transmissions," in "ECOC 2016; 42nd European Conference on Optical Communication; Proceedings of," (VDE, 2016), pp. 1–3.
27. S. T. Le, I. D. Phillips, J. E. Prilepsky, M. Kamalian, A. D. Ellis, P. Harper, and S. K. Turitsyn, "Achievable information rate of nonlinear inverse synthesis based 16QAM OFDM transmission," in "ECOC 2016; 42nd European Conference on Optical Communication; Proceedings of," (VDE, 2016), pp. 1–3.
28. S. T. Le, K. Schuh, F. Buchali, and H. Bülow, "100 Gbps b-modulated nonlinear frequency division multiplexed transmission," in "Optical Fiber Communication Conference," (Optical Society of America, 2018), pp. W1G–6.
29. Z. Dong, S. Hari, T. Gui, K. Zhong, M. Yousefi, C. Lu, P.-K. A. Wai, F. Kschischang, and A. Lau, "Nonlinear frequency division multiplexed transmissions based on NFT," IEEE Photon. Technol. Lett. pp. 1–1 (2015).
30. T. Gui, T. H. Chan, C. Lu, A. P. T. Lau, and P.-K. A. Wai, "Alternative decoding methods for optical communications based on nonlinear Fourier transform," J. Lightw. Technol. **35**, 1542–1550 (2017).
31. T. Gui, C. Lu, A. P. T. Lau, and P. Wai, "High-order modulation on a single discrete eigenvalue for optical communications based on nonlinear Fourier transform," Opt. express **25**, 20286–20297 (2017).
32. S. T. Le, J. E. Prilepsky, and S. K. Turitsyn, "Nonlinear inverse synthesis for high spectral efficiency transmission in optical fibers," Opt. Express **22**, 26720–26741 (2014).
33. S. Civelli, L. Barletti, and M. Secondini, "Numerical methods for the inverse nonlinear Fourier transform," in "Digital Communications (TIWDC), 2015 Tyrrhenian International Workshop on," (IEEE, 2015), pp. 13–16.
34. G. Boffetta and A. R. Osborne, "Computation of the direct scattering transform for the nonlinear Schroedinger equation," J. Comput. Phys. **102**, 252–264 (1992).
35. A. Mecozzi, C. Antonelli, and M. Shtaif, "Coupled Manakov equations in multimode fibers with strongly coupled groups of modes," Opt. express **20**, 23436–23441 (2012).
36. G. P. Agrawal, *Nonlinear Fiber Optics* (Academic, San Diego, CA, 2001), 3rd ed.
37. S. Mumtaz, R.-J. Essiambre, and G. P. Agrawal, "Nonlinear propagation in multimode and multicore fibers: generalization of the Manakov equations," J. Lightw. Technol. **31**, 398–406 (2013).
38. A. Aricò, G. Rodriguez, and S. Seatzu, "Numerical solution of the nonlinear Schrödinger equation, starting from the scattering data," Calcolo **48**, 75–88 (2011).
39. S. Civelli, E. Forestieri, and M. Secondini, "Why noise and dispersion may seriously hamper nonlinear frequency-division multiplexing," IEEE Photon. Technol. Lett. **29**, 1332–1335 (2017).
40. R. A. Shafik, M. S. Rahman, and A. R. Islam, "On the extended relationships among EVM, BER and SNR as performance metrics," in "Electrical and Computer Engineering, 2006. ICECE'06. International Conference on," (IEEE, 2006), pp. 408–411.
41. S. A. Derevyanko, J. E. Prilepsky, and S. K. Turitsyn, "Capacity estimates for optical transmission based on the nonlinear Fourier transform," Nat. Commun. **7**, 12710 (2016).
42. I. Tavakkolnia and M. Safari, "Dispersion pre-compensation for NFT-based optical fiber communication systems," in "Conference on Lasers and Electro-Optics, OSA Technical Digest," (2016).
43. S. Civelli, E. Forestieri, and M. Secondini, "Precompensation and windowing for nonlinear frequency-division multiplexing," in "Progress In Electromagnetics Research Symposium - Spring (PIERS) 2017," (2017).

Optics EXPRESS

44. S. Civelli, E. Forestieri, and M. Secondini, "A novel detection strategy for nonlinear frequency-division multiplexing," in "Optical Fiber Communication Conference," (Optical Society of America, 2018), pp. W1G–5.
45. S. Civelli, E. Forestieri, and M. Secondini, "Decision-feedback detection strategy for nonlinear frequency-division multiplexing," Opt. Express **26**, 12057–12071 (2018).

1. Introduction

The exponential increase in global data traffic is constantly challenging the capability of current-generation optical fiber communication systems to meet the data rate demand [1, 2]. To address the future capacity needs of optical fiber networks and forestall the infamous "capacity crunch" problem [1], two solutions have been widely considered: space division multiplexing (SDM), implying the installation of new multimode or multicore fibers in place of current-generation fibers, or simply to extensively increase the number of conventional single-mode fibers. Both approaches have to face serious problems in terms of deployment costs. On the other hand, because of the huge number of already installed fibers and the obvious engineers' goal to maximize the information rate for every available spatial dimension (fiber, core, or mode), there exists a great interest in the compensation, mitigation [3], or constructive use of fiber nonlinearity [4]. The nonlinearity of optical fiber systems is believed to be the main limiting factor deteriorating the performance at high signal powers [1, 2]. In the past years, some novel approaches based on the nonlinear Fourier transform (NFT) [5–7] have been actively investigated in order to master the fiber nonlinearity and, eventually, to pave the way for going beyond the nonlinearity-imposed limits of linear transmission techniques [4, 8, 9]. The NFT, which can be thought of as a nonlinear analog of the conventional Fourier transform (FT), is a mathematical tool to solve a class of nonlinear differential equations, including the nonlinear Schrödinger equation (NLSE) [5] and Manakov equation [10], both serving as general master models governing the propagation of optical signals along the fiber. The NFT decomposes a signal into a set of both discrete and continuous spectral components, the so-called nonlinear spectrum, that evolves in a simple linear way along the essentially nonlinear fiber channel. Nonlinear frequency-division multiplexing (NFDM) [4, 9, 11–18, and reference therein] is an optical fiber transmission technique in which we encode the information on the nonlinear (NFT) spectrum, such that, differently from conventional wavelength division multiplexing (WDM), the different users are assigned different domains ("bands") in the NFT spectrum. The latter evolves linearly along the fiber, which guarantees the absence of crosstalk between users (responsible for a severe performance degradation in WDM systems) and the possibily to exactly remove propagation effects by simple processing. These characteristics make the NFDM a good candidate for the next generation of fiber systems, taking into account inherent robustness to fiber nonlinearity and the potential to outperform conventional "nonlinearity-degraded" systems.

Until recently, the NFT-based transmission has been mostly considered in the single-polarization case and, hence, based on the NFT processing associated with the NLSE channel ($\mathrm{NFT}_{\mathrm{NLS}}$). However, the standard single mode fiber (SSMF) supports two orthogonal propagation modes and high-efficiency transmission methods typically use both polarization components for modulation. Under some fully realistic conditions, the averaged dynamics of two orthogonal modes in randomly-birefringent fibers (at distances much longer that the polarization mixing scale) is governed by the integrable version of the Manakov equation (ME) [19], whose NFT form has been known since the original paper by Manakov [10]. The possibility to double the transmission rate of NFT-based systems by employing both polarization components had remained almost unexplored until 2017 aside, perhaps, from just one earlier work [20]. At the same time, the need of incorporating both polarization components into NFT-based systems is apparent, such that, more recently, joint polarization and nonlinear frequency-division multiplexing (PNFDM) schemes have been gradually getting more attention [20–25].

Finally, we also mention the considerable progress achieved over the past several years in the

Optics EXPRESS

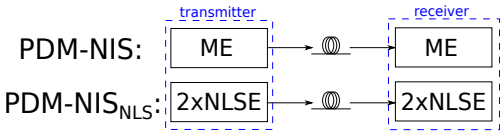

Fig. 1. Details of NFT processing in PDM-NIS (above) and PDM-NIS$_{NLS}$ (below).

experimental demonstration and analysis of NFDM optical transmission systems. Experimental demonstrations of single-polarization NFDM systems were performed independently by several groups [12, 13, 15, 16, 26–31]. More recently, also PNFDM schemes have been experimentally demonstrated, using either the discrete [22, 23] or continuous spectrum [25].

In this paper we introduce the polarization division multiplexing nonlinear inverse synthesis (PDM-NIS), the dual polarization analog of the nonlinear inverse synthesis (NIS) scheme that was initially proposed for the NLSE in [18, 32]. Within the NIS we are to synthesize the time-domain profile starting from the given encoded nonlinear spectrum (its continuous part), similarly to the method widely used for Bragg gratings profile synthesis. So the NIS allows us to directly combine the efficient modulation formats borrowed from "linear" transmission methods with the NFT-based processing. The synthesis operation can be done by solving Gelfand-Levitan-Marchenko equations, i.e. by the inverse NFT (INFT) at the transmitter (TX) side. In this paper we basically use the same original NIS idea but working with the dual-polarization channel. After a brief summary concerning the NFT for the ME (NFT$_{M}$), we present the generalization of some numerical algorithms (originally devised for the scalar NFT [33, 34]) to the case of the ME. The proposed algorithms are very general, i.e., they can be applied to any number of symmetrically-coupled NLSE-type equations, meaning the possibility of their direct application to SDM-NFT systems, where the signal propagation is governed by the vector NLSE (VNLSE) under some realistic conditions [35]. Then the PDM-NIS system is described and its performance is studied and compared with the performance of single-polarization NIS systems. Further on, we propose and investigate a simplified approach to PDM-NIS based on scalar NFT processing: instead of applying the more complex NFT$_{M}$—the NFT approach based on the ME for encoding and decoding information on the nonlinear spectrum, as sketched in the upper part of Fig. 1—we propose to use an independent NFT$_{NLS}$ processing, based on the NLSE channel, for each polarization component of the signal. The PDM-NIS$_{NLS}$ scheme, using the latter simplified processing, is sketched in the lower part of Fig. 1. We demonstrate that, in a certain range of system parameters, where performance is dominated by the effect of noise on the nonlinear spectrum, such a reduced complexity processing can even provide a performance improvement compared to the full vector processing, in spite of the mismatch between channel model and processing.

2. Manakov equation and the nonlinear Fourier transform

It is well known that due to inhomogeneities, the conventional SSMFs are birefringent and support two orthogonal modes that can generally have a different group velocity. Birefringence randomly varies both in magnitude and direction along the fiber, causing a phenomenon known as polarization mode dispersion (PMD) [36]. Averaging over the rapidly varying birefringence yields the Manakov-PMD equation [19]. Considering typical optical fibers used in communication systems and neglecting linear PMD effects and loss (i.e., assuming path-average model), the Manakov-PMD equation in the leading order reduces to the integrable ME [19]

$$j\frac{\partial \mathbf{Q}}{\partial X} = \frac{\beta_2}{2}\frac{\partial^2 \mathbf{Q}}{\partial T^2} - \gamma\frac{8}{9}||\mathbf{Q}||^2\mathbf{Q}, \tag{1}$$

Optics EXPRESS

where $\mathbf{Q} = (Q_1, Q_2)$ is the two-component electric field envelope, X is the coordinate along the fiber, T is the retarded time, β_2 is the group velocity dispersion (GVD) parameter, and γ is the nonlinear Kerr parameter. Note that if the initial pulse is set on a single polarization as $\mathbf{Q} = (Q_1, 0)$, the averaged ME reduces further to the NLSE form.

Considering the same normalization procedure as in [21], Eq. (1) turns into the normalized ME

$$j\frac{\partial \mathbf{q}}{\partial x} = \frac{\partial^2 \mathbf{q}}{\partial t^2} + 2\sigma||\mathbf{q}||^2\mathbf{q}, \tag{2}$$

where $\sigma = -\mathrm{sgn}(\beta_2)$ (we further consider only the case of anomalous dispersion: $\sigma = 1$). Moreover, if $\mathbf{q}$ is a multidimensional vector, Eq. (2) is the VNLSE, master model for the propagation in multimode and multicore fibers in the strong coupling regime [35,37]. Importantly, the VNLSE is solvable with the NFT method [7, 10]. In the following we briefly present the NFT for the VNLSE of dimension M, which reduces to ME for $M = 2$, and to the scalar NLSE for $M = 1$.

The direct $\mathrm{NFT_M}$ operation consists in decomposing the normalized M-dimensional optical signal $\mathbf{q}(t)$ into its nonlinear spectral components. This is achieved by solving the $M + 1$-component Zakharov-Shabat problem [7, 10], as detailed in Section 3 below. As usual, the nonlinear (NFT) spectrum of any localized signal (having a finite L_1-norm) is composed of the continuous part, describing the dispersive radiation, and the discrete part, corresponding to non-dispersive modes—solitons. The continuous NFT spectrum is given by the M-component reflection coefficient

$$\boldsymbol{\rho}(\lambda) = \mathbf{b}(\lambda)/a(\lambda) \tag{3}$$

where $a(\lambda)$ and $\mathbf{b}(\lambda)$ are the scattering data obtained from the solution of the Zakharov-Shabat problem, with $\mathbf{b}(\lambda)$ being a row vector of dimension M. The discrete part, if present, consists of some number N of discrete eigenvalues $\{\lambda_i\}_{i=1}^N$—corresponding to the zeros of $a(\lambda)$ in the upper complex half-plane of λ—and the corresponding M-component complex-valued norming constants $\{\mathbf{C}_i\}_{i=1}^N$. For a simple zero λ_i, the norming constants can be expressed as

$$\mathbf{C}_i = \mathbf{b}(\lambda_i)/a'(\lambda_i). \tag{4}$$

The inverse operation to retrieve the time domain signal from the nonlinear spectrum, $\mathrm{INFT_M}$, can be performed via the solution of the M-dimensional Gelfand-Levitan-Marchenko equation (GLME), i.e., the vector GLME (VGLME), associated with Eq. (2) [7]

$$\mathbf{K}(x, y) - \sigma\mathbf{F}^{\dagger}(x + y) + \sigma\int_x^{\infty}\int_x^{\infty}\mathbf{K}(x, r)\mathbf{F}(r + s)\mathbf{F}^{\dagger}(s + y)\, ds dr = 0, \tag{5}$$

written here for the unknown M-component function $\mathbf{K}(x, y)$. Here and in the following $\dagger$ indicates complex conjugate and transposed (i.e. the Hermitian conjugation), while * indicates complex conjugate (without the transposition). The M-dimensional kernel function $\mathbf{F}(x)$ in (5) depends on the NFT spectrum and, if all the zeros λ_i of $a(\lambda)$ are simple, is expressed as

$$\mathbf{F}(x) = \frac{1}{2\pi}\int_{-\infty}^{+\infty}\boldsymbol{\rho}(\lambda)e^{j\lambda x}\, d\lambda - j\sum_{i=1}^{N}\mathbf{C}_i e^{j\lambda_i x}. \tag{6}$$

Finally, the time domain signal is obtained as $\mathbf{q}(x) = -2\mathbf{K}(x, x)$ [7]. The propagation of the nonlinear spectrum to normalized distance $\mathcal{L}$ is equivalent to the multiplication of each NFT spectral component by $e^{-4j\lambda^2\mathcal{L}}$.

The presentation given above applies to ME for $\mathbf{q}(t) = (q_1(t), q_2(t))$ when $M = 2$. In this case,

$$\mathbf{b}(\lambda) = (b_1(\lambda), b_2(\lambda)) \tag{7}$$

Optics EXPRESS

and the dual components nonlinear spectrum is

$$\boldsymbol{\rho}(\lambda) = \big(\rho_1(\lambda), \rho_2(\lambda)\big) = \big(b_1(\lambda)/a(\lambda), b_2(\lambda)/a(\lambda)\big) \tag{8}$$

$$\mathbf{C}_i = \big(b_1(\lambda_i)/a'(\lambda_i), b_2(\lambda_i)/a'(\lambda_i)\big). \tag{9}$$

The following normalization condition holds for any $\lambda \in \mathbb{R}$:

$$|a(\lambda)|^2 + \sigma|b_1(\lambda)|^2 + \sigma|b_2(\lambda)|^2 = 1. \tag{10}$$

The nonlinear analog of Parseval's identity that relates the energy of time domain signal to the energy defined through the nonlinear spectrum, is as follows

$$\int_{-\infty}^{+\infty} |q_1(t)|^2 + |q_2(t)|^2\, dt = 4\sum_{k=1}^{N} \Im\{\lambda_k\} + \frac{\sigma}{\pi}\int_{-\infty}^{+\infty} \log(1 + \sigma|\rho_1(\lambda)|^2 + \sigma|\rho_2(\lambda)|^2)\, d\lambda. \tag{11}$$

Finally, an important property of the NFT states that if R is a unitary 2×2 matrix, i.e., $R^\dagger R = I$, than

$$\mathrm{NFT_M}\,(R\mathbf{q}) = R^*\mathrm{NFT_M}\,(\mathbf{q})\,. \tag{12}$$

This property, which is not true in general for any matrix R, can be proved through the direct NFT, as shown at the end of Subsection 3.1. A similar property for the NFT associated with the scalar NFT was proved in [9].

3. Numerical methods for NFT and INFT computation in vector NLSE

In the following subsections we describe two numerical algorithms for the computation of the NFT and INFT operations, explicitly considering the VNLSE Eq. (2), for the M-dimensional vector signal $\mathbf{q}(t) = (q_1(t), \ldots, q_M(t))$. Recall that, when $M = 2$ the VNLSE reduces to the ME, while for $M = 1$ it becomes the NLSE. Hence, the following methods are general and applicable also to SDM-NFT systems, though the details of their optimization is beyond the scope of our work.

In the following, we indicate with $\mathbf{I}_K$ the $K \times K$ identity matrix, $\mathbf{0}_{K\times G}$ the $K \times G$ matrix with all zero entries. Vectors are indicated with bold characters, while their components are indicated in non-bold with subscripts, e.g., $\mathbf{v} = (v_1, \ldots, v_N)$ is a row vector of length N, whose k-th component is v_k. Also, empty spaces in matrices correspond to zero components.

3.1. Direct NFT

In this subsection we present a numerical method to recover the scattering data $a(\lambda)$ and $\mathbf{b}(\lambda)$ (recall that our $\mathbf{b}$ is now an M-dimensional vector) starting from the time domain signal $\mathbf{q}(t)$, i.e. to solve the vector Zakharov-Shabat problem associated with the VNLSE [7]. The method considered here is a multidimensional extension of the Boffetta-Osborne method [34] (also known as the layer-peeling method [9, Part II]) developed for the scalar NLSE.

The eigenvalue problem for the VNLSE [7] is written as $\boldsymbol{\nu}_t = P\boldsymbol{\nu}$, where $\boldsymbol{\nu} \in \mathbb{C}^{M+1\times 1}$ is an auxiliary $M + 1$-dimensional function, and

$$P = \begin{pmatrix} -j\lambda & q_1(t) & \ldots & q_M(t) \\ -\sigma q_1^*(t) & j\lambda & & \\ \vdots & & \ddots & \\ -\sigma q_M^*(t) & & & j\lambda \end{pmatrix} \tag{13}$$

Optics EXPRESS

an $M+1\times M+1$ coupling matrix containing the signal $\mathbf{q}(t)$ as an effective potential. The solutions of of $\boldsymbol{\nu}_t = P\boldsymbol{\nu}$ fixed by the boundary conditions at either the trailing or leading end of the multidimensional pulse have the basis [7]:

$$\overbrace{\boldsymbol{\phi}(t,\lambda)\sim\begin{pmatrix}1\\ \mathbf{0}_{M\times 1}\end{pmatrix}e^{-j\lambda t}}^{M+1\times 1},\quad \overbrace{\bar{\boldsymbol{\phi}}(x,\lambda)\sim\begin{pmatrix}\mathbf{0}_{1\times M}\\ \mathbf{I}_M\end{pmatrix}e^{j\lambda t}}^{M+1\times M}\quad \text{as } t\to-\infty, \tag{14}$$

$$\underbrace{\boldsymbol{\psi}(t,\lambda)\sim\begin{pmatrix}\mathbf{0}_{1\times M}\\ \mathbf{I}_M\end{pmatrix}e^{j\lambda t}}_{M+1\times M},\quad \underbrace{\bar{\boldsymbol{\psi}}(x,\lambda)\sim\begin{pmatrix}1\\ \mathbf{0}_{M\times 1}\end{pmatrix}e^{-j\lambda t}}_{M+1\times 1}\quad \text{as } t\to+\infty. \tag{15}$$

The scattering data $a(\lambda)$ and $\mathbf{b}(\lambda)$ can be defined expressing $\boldsymbol{\phi}$ through $\{\boldsymbol{\psi},\bar{\boldsymbol{\psi}}\}$, similarly to what we have in the NLSE case [4, 7]

$$\boldsymbol{\phi}(t,\lambda)=\boldsymbol{\psi}(t,\lambda)\mathbf{b}(\lambda)+\bar{\boldsymbol{\psi}}(t,\lambda)a(\lambda). \tag{16}$$

The scattering coefficients can further be obtained through the evaluation of the solution $\boldsymbol{\phi}(t,\lambda)$, defined by the boundary condition at $-\infty$, at the opposite end of the interval

$$a(\lambda)=\lim_{t\to+\infty}\phi_1(t,\lambda)e^{+j\lambda t},\qquad b_m(\lambda)=\lim_{t\to+\infty}\phi_{m+1}(t,\lambda)e^{-j\lambda t}, \tag{17}$$

for $m=1,\dots,M$.

Let us assume that $|\mathbf{q}(t)|=0$ for $|t|>T$ and consider a uniform grid with $t_n=-T+(n-1)\delta$ for $n=1,\dots,N_t+1$, and discretization step $\delta=2T/N_t$. The idea is to iteratively solve the Cauchy problem,

$$\begin{cases}\boldsymbol{\phi}_t=P^{(n)}\boldsymbol{\phi} & \text{for } t\in(t_n-\delta/2,t_n+\delta/2],\\ \boldsymbol{\phi}(t_n-\delta/2)=\boldsymbol{\phi}^{(n)} & \text{boundary condition,}\end{cases} \tag{18}$$

to define the boundary condition for the following iteration as $\boldsymbol{\phi}^{(n+1)}=\boldsymbol{\phi}(t_n+\delta/2)$. The matrix $P^{(n)}$ is obtained from P by considering a piece-wise constant approximation for $\mathbf{q}(t)$, i.e., assuming that $\mathbf{q}(t)\simeq\mathbf{q}^{(n)}$ for $t\in(t_n-\delta/2,t_n+\delta/2]$, with $\mathbf{q}^{(n)}\triangleq\mathbf{q}(t_n)$. The starting point, given by the boundary condition for $\boldsymbol{\phi}(t,\lambda)$ in $t=-T-\delta/2$, is

$$\boldsymbol{\phi}^{(1)}=\begin{pmatrix}1\\ \mathbf{0}_{M\times 1}\end{pmatrix}e^{j\lambda(T+\delta/2)}. \tag{19}$$

The scattering data are obtained from the end point solution as $a(\lambda)=\phi_1^{(N_t+1)}e^{+j\lambda(T+\delta/2)}$ and $b_m(\lambda)=\phi_{m+1}^{(N_t+1)}e^{-j\lambda(T+\delta/2)}$, for $m=1,\dots,M$.

The solution of the Cauchy problem (18) is obtained by using the transfer-matrix approach [4]. For each iteration (elementary step in t) we have $\boldsymbol{\phi}^{(n+1)}=U^{(n)}\boldsymbol{\phi}^{(n)}$, where $U^{(n)}=\exp(P^{(n)}\delta)$ is the transfer matrix. Using the definition of matrix exponential, the Taylor expansion for sinh and cosh functions, and doing some straightforward calculations, we obtain the following expression for the single-step transfer matrix

$$U^{(n)}=\left(\begin{array}{c|ccc}c_0-j\lambda s_0 & q_1^{(n)}s_0 & \dots & q_M^{(n)}s_0\\ \hline -\sigma q_1^{(n)*}s_1 & c_1+j\lambda s_1 & & \\ \vdots & & \ddots & \\ -\sigma q_M^{(n)*}s_M & & & c_M+j\lambda s_M\end{array}\right), \tag{20}$$

Optics EXPRESS

where $c_k = \cosh(\delta d_k)$ and $s_k = \sinh(\delta d_k)/d_k$ for $k = 0, 1, \ldots, M$, with

$$d_0 = \sqrt{-\lambda^2 - \sigma \sum_{k=1}^{M} |q_k^{(n)}|^2} \quad \text{and} \quad d_k = \sqrt{-\lambda^2 - \sigma |q_k^{(n)}|^2} \tag{21}$$

for $k = 1, \ldots, M$. Finally, the desired multidimensional scattering data for the VNLSE (defining our NFT spectrum) can be obtained as

$$\begin{cases} a(\lambda) = \Sigma_1 e^{j\lambda(2T+\delta)}, \\ b_m(\lambda) = \Sigma_{m+1}, \end{cases} \quad \text{for } m = 1, \ldots, M, \text{ where } \quad \mathbf{\Sigma} = U^{(N_t+1)} \cdots U^{(1)} \begin{pmatrix} 1 \\ \mathbf{0}_{M\times 1} \end{pmatrix} \in \mathbb{C}^{M+1\times 1} \tag{22}$$

Moreover, denoting by the prime the derivative with respect to λ, $a'(\lambda)$ (which is used for the computation of the norming constants) is obtained as

$$a'(\lambda) = \phi_1^{\prime(N_t+1)} e^{j\lambda 2T} \tag{23}$$

where $\boldsymbol{\phi}^{\prime(N_t+1)}$ is computed from the recursion

$$\boldsymbol{\phi}^{\prime(n+1)} = U^{(n)} \boldsymbol{\phi}^{\prime(n)} + U^{\prime(n)} \boldsymbol{\phi}^{(n)}, \tag{24}$$

where

$$U^{\prime(n)} = \left(\begin{array}{c|ccc} j\lambda^2\delta/d_0^2 c_0 - \Gamma_0 s_0 & -q_1^{(n)}\lambda/d_0^2(\delta c_0 - s_0) & \cdots & -q_M^{(n)}\lambda/d_0^2(\delta c_0 - s_0) \\ \hline \sigma q_1^{(n)*}\lambda/d_1^2(\delta c_1 - s_1) & -j\lambda^2\delta/d_1^2 c_1 + \Gamma_1 s_1 & & \\ \vdots & & \ddots & \\ \sigma q_M^{(n)*}\lambda/d_M^2(\delta c_M - s_M) & & & -j\lambda^2\delta/d_M^2 c_M + \Gamma_M s_M \end{array} \right), \tag{25}$$

$\Gamma_0 = (\lambda\delta + j + j\lambda^2/d_0^2)$, and $\Gamma_m = (-\lambda\delta + j + j\lambda^2/d_m^2)$ for $m = 1, \ldots, M$. The recursion (24) is initialized by setting $\boldsymbol{\phi}^{\prime(1)} = (0, \ldots, 0)^{\mathrm{T}}$.

To demonstrate Eq. (12) for $M = 2$ it is enough to prove that if $\mathbf{v}$ solves the Zakarov-Shabat problem $\mathbf{v}_t = P(\mathbf{q})\mathbf{v}$ where $P(\mathbf{q})$ is the matrix (13) associated with the potential $\mathbf{q}$, than a solution of the Zakarov-Shabat problem associated with the potential $R\mathbf{q}$ is

$$\mathbf{u} := \mathcal{R}\mathbf{v} = \begin{pmatrix} 1 & 0 & 0 \\ 0 & R_{11}^* & R_{12}^* \\ 0 & R_{21}^* & R_{22}^* \end{pmatrix} \mathbf{v}, \tag{26}$$

i.e., $\mathbf{u}_t = P(R\mathbf{q})\mathbf{u}$. This property can be proved using $\mathbf{v}_t = P(\mathbf{q})\mathbf{v}$ and the properties of R. Consequently, $\mathcal{R}\boldsymbol{\phi}$ has the same boundary condition as $\boldsymbol{\phi}$ and solves $\mathbf{u}_t = P(R\mathbf{q})\mathbf{u}$ and, thus, the scattering data and the nonlinear spectrum can be obtained from its values at $+\infty$. The first component, which represents $a(\lambda)$, does not change, while the second and the third components, which represent $b_1(\lambda)$ and $b_2(\lambda)$, change with R^*. Consequently, the nonlinear spectrum $\rho(\lambda)$ also changes according to multiplication by R^*. In mathematical formulas

$$\boldsymbol{\rho}_R(\lambda) = \mathbf{b}_R(\lambda)/a_R(\lambda) = R^*\mathbf{b}(\lambda)/a(\lambda) = R^*\boldsymbol{\rho}(\lambda), \tag{27}$$

where the subscript $_R$ indicates that the quantity is related to the potential $R\mathbf{q}$, rather than $\mathbf{q}$.

Optics EXPRESS

3.2. Inverse NFT

In this subsection, we derive the Nystrom-conjugate gradient method to compute the INFT for the VNLSE, generalizing the concepts used for the NLSE in [33, 38]. Up to our knowledge, two numerical methods for the INFT for VNLSE are available: the authors of [21] proposed to invert the direct NFT method, when the discrete nonlinear spectrum is absent, while the authors of [22] presented a generalized Darboux transform to recover the optical signal from the discrete spectrum, when the continuous spectrum is absent. On the other hand, the method presented here is more general, as it applies to the VGLME of arbitrary dimension M and can be used in presence of both the discrete and continuous spectrum.

Firstly, let us define the Hankel matrices and describe a method to perform fast matrix multiplications when dealing with them. An upper left triangular Hankel matrix $\mathcal{H}$ of dimension $N_{\mathcal{H}} \times N_{\mathcal{H}}$, generated by the vector $\mathbf{h} = (h_1, \ldots, h_{N_{\mathcal{H}}})$, is the matrix of the form:

$$\mathcal{H} = \mathcal{H}(\mathbf{h}) = \begin{pmatrix} h_1 & h_2 & h_3 & \ldots & h_{N_{\mathcal{H}}} \\ h_2 & h_3 & \ldots & h_{N_{\mathcal{H}}} & 0 \\ h_3 & \ldots & h_{N_{\mathcal{H}}} & & \vdots \\ \ldots & h_{N_{\mathcal{H}}} & & & \\ h_{N_{\mathcal{H}}} & 0 & \ldots & & 0 \end{pmatrix}, \tag{28}$$

having $\mathbf{h}$ as first row and $\mathbf{h}^{\mathrm{T}}$ as first column. The circulant matrix of dimension $N_C \times N_C$ generated by the vector $\mathbf{c} = (c_1, \ldots, c_{N_C})$ is the matrix

$$C(\mathbf{c}) = \begin{pmatrix} c_1 & c_2 & c_3 & \ldots & c_{N_C} \\ c_{N_C} & c_1 & c_2 & \ldots & \vdots \\ c_{N_C-1} & c_{N_C} & c_1 & \ldots & c_3 \\ \vdots & \ddots & \ddots & \ddots & c_2 \\ c_2 & \ldots & c_{N_C-1} & c_{N_C} & c_1 \end{pmatrix}, \tag{29}$$

having $\mathbf{c}$ as first row and $\tilde{\mathbf{c}} = (c_1, c_{N_C}, \ldots, c_2)^{\mathrm{T}}$ as first column.

The product of the matrix $\mathcal{H}$ for a column vector $\mathbf{x}$ of length $N_{\mathcal{H}}$ can be performed considering the first $N_{\mathcal{H}}$ components resulting from the product of the circulant matrix of doubled dimensions $C = C(\mathbf{h}_0)$ generated by the vector $\mathbf{h}_0 = (\mathbf{h}, \mathbf{0}_{1\times N_{\mathcal{H}}})$ with the vector $\mathbf{x}_0 = (\mathbf{x}^{\mathrm{T}}, \mathbf{0}_{1\times N_{\mathcal{H}}})^{\mathrm{T}}$. Specifically, if $C(\mathbf{h}_0)\mathbf{x}_0 = \mathbf{y}_0 = (\mathbf{y}^{\mathrm{T}}, \mathbf{w}^{\mathrm{T}})^{\mathrm{T}}$ where both $\mathbf{y}$ and $\mathbf{w}$ are column vector of $N_{\mathcal{H}}$ components, then $\mathbf{y} = \mathcal{H}\mathbf{x}$. The product $\mathbf{y}_0 = C(\mathbf{h}_0)\mathbf{x}_0$ is the discrete circular convolution between the vectors $\tilde{\mathbf{h}}_0$, where $\tilde{\mathbf{h}}_0^{\mathrm{T}} = (h_1, \mathbf{0}_{1\times N_{\mathcal{H}}}, h_{N_{\mathcal{H}}}, \ldots, h_2)^{\mathrm{T}}$, and $\mathbf{x}_0$, and therefore can be efficiently computed numerically through the FFT operations as IFFT(FFT($\tilde{\mathbf{h}}_0$)·FFT($\mathbf{x}_0$)), where · indicates point to point multiplication.

The INFT is computed by solving the VGLME, Eq. (5), of dimension $1 \times M$. This equation can be rewritten as the Marchenko system of order $M + 1$:

$$\begin{cases} B_1(t,\alpha) - \sigma \int_0^{+\infty} \mathbf{B}_2(t,\beta)\mathbf{F}(\alpha+\beta+2t)\, d\beta = 0 & \text{scalar equation,} \\ \mathbf{B}_2(t,\alpha) - \sigma\mathbf{F}^{\dagger}(\alpha+2t) + \int_0^{+\infty} B_1(t,\beta)\mathbf{F}^{\dagger}(\alpha+\beta+2t)\, d\beta = 0 & M \text{ coupled equations,} \end{cases} \tag{30}$$

where $B_1(x,\alpha)$ is a scalar unkown function and $\mathbf{B}_2(x,\alpha)$ is a vector of $1 \times M$ unkown functions. The time domain signal (of M components) is obtained as $\mathbf{q}(t) = -2\mathbf{B}_2(t,0)$.

Assuming that $|\mathbf{q}(t)| = 0$ for $|t| > T$, consider the uniform grid over the interval $[-T, T]$, with $t_k = -T + (k-1)\delta$ for $k = 1, \ldots, N_t + 1$ and time step $\delta = 2T/N_t$. For each $t_k \in [-T, T]$, the solution $\mathbf{q}(t_k) = -2\mathbf{B}_2(t_k, 0)$ depends on the values of $\mathbf{F}(\alpha+\beta+2t_k)$, $\mathbf{B}_2(t_k,\beta)$, and $B_1(t_k,\beta)$ for $\alpha, \beta \geq 0$, as clear from Eq. (30). Therefore, we shall consider a uniform grid for α and

Optics EXPRESS

β in the interval $[0, T_B)$ (given T_B such that $|\mathbf{F}(y)| = 0$ for $y \geq 2t_k + T_B$, and $|B_1(t_k, \alpha)| = 0$ and $|\mathbf{B}_2(t_k, \alpha)| = 0$ for $\alpha \geq T_B$) with discretization step 2δ: $\alpha_\ell = (l-1)2\delta$ and $\beta_\ell = (\ell-1)2\delta$ for $\ell = 1, \ldots, L$, with $L = \lceil T_B/(2\delta) \rceil$. Using the Nystrom method, the Marchenko system in Eq. (30) can be reduced to a linear system, discretizing the integrals through the composite Simpson's quadrature rule. The composite Simpson's quadrature rule numerically integrates the function $f(x)$ in $[a, b]$, applying the Simpson's rule on n sub-intervals of width $\Delta = (b-a)/n$. If $x_k = a + (k-1)\Delta$ for $k = 1, \ldots, n+1$, the integral value is approximated as

$$\int_a^b f(x)\,dx \approx \frac{\Delta}{3}\left[f(x_1) + 4\sum_{j=1}^{n/2} f(x_{2j}) + 2\sum_{j=1}^{n/2-1} f(x_{2j+1}) + f(x_{n+1})\right], \tag{31}$$

i.e., the values of $f(x)$ on the grid $x_1, \ldots, x_{n+1}$ of $[a, b]$ are numerically integrated with the weights $\mathbf{d} = \Delta/3(1, 4, 2, 4, \ldots, 4, 2, 4, 1)$.

The linear system equivalent to (30) is

$$\underbrace{\left(\begin{array}{c|ccc} \mathbf{I}_L & -\sigma H_1 D & \ldots & -\sigma H_M D \\ \hline H_1^* D & & & \\ \vdots & & \mathbf{I}_{LM} & \\ H_M^* D & & & \end{array}\right)}_{L(M+1)\times L(M+1)} \underbrace{\left(\begin{array}{c} \mathbf{b}_1 \\ \mathbf{b}_{2,1} \\ \vdots \\ \mathbf{b}_{2,M} \end{array}\right)}_{L(M+1)\times 1} = \underbrace{\left(\begin{array}{c} \mathbf{0}_{L\times 1} \\ \sigma\mathbf{f}_1^* \\ \vdots \\ \sigma\mathbf{f}_M^* \end{array}\right)}_{L(M+1)\times 1}, \tag{32}$$

where D is the $L \times L$ diagonal matrix that defines the quadrature rule according to $D_{\ell,\ell} = d_\ell$ for $\ell = 1, \ldots, L$; $\mathbf{b}_1$ and $\mathbf{b}_{2,m}$ are the $L \times 1$ vectors containing, respectively, the values of $B_1(t_k, \alpha)$ and $\mathbf{B}_{2,m}(t_k, \alpha)$, i.e., $b_{1\ell} = B_1(t_k, \alpha_\ell)$ and $b_{2,m,\ell} = B_{2,m}(t_k, \alpha_\ell)$ for $\ell = 1, \ldots, L$; H_m is the $L \times L$ matrix containing the values of $F_m(\alpha + \beta + 2t_k)$ with $H_{m,\ell,g} = F_m(\alpha_\ell + \alpha_g + 2t_k)$ for $\ell, g = 1, \ldots, L$; and $\mathbf{f}_m$ is the vector $L \times 1$ containing the values of $F_m(\alpha + 2t_k)$ with $f_{m,\ell} = F_m(\alpha_\ell + 2t_k)$ for $\ell = 1, \ldots, L$. Importantly, $\mathbf{f}_m$ is the first row of the matrix H_m, and H_m is the triangular upper left Hankel matrix generated by the vector $\mathbf{f}_m$.

Eq. (32) can be equivalently written in a compact form as

$$\underbrace{\left(\begin{array}{cc} \mathbf{I}_L & -\sigma\mathbf{H}\mathbf{D}_{LM} \\ \mathbf{H}^\dagger D & \mathbf{I}_{LM} \end{array}\right)}_{L(M+1)\times L(M+1)} \underbrace{\left(\begin{array}{c} \mathbf{b}_1 \\ \mathbf{b}_2 \end{array}\right)}_{L(M+1)\times 1} = \underbrace{\left(\begin{array}{c} \mathbf{0}_{L\times 1} \\ \sigma\mathbf{f}^\dagger \end{array}\right)}_{L(M+1)\times 1}, \tag{33}$$

where $\mathbf{H} = (H_1, \ldots, H_m)$ is an $L \times LM$ matrix, $\mathbf{f} = (\mathbf{f}_1^{\mathrm{T}}, \ldots, \mathbf{f}_m^{\mathrm{T}})^{\mathrm{T}}$ is a $LM \times 1$ vector, $\mathbf{b}_2 = (\mathbf{b}_1^{\mathrm{T}}, \ldots, \mathbf{b}_M^{\mathrm{T}})^{\mathrm{T}}$ is a $LM \times 1$ vector, and $\mathbf{D}_{LM}$ is the $LM \times LM$ diagonal matrix with diagonal $(\mathbf{d}, \ldots, \mathbf{d})$. Substituting the first row into the second and multiplying by $\mathbf{D}_{LM}$, we obtain the system of LM equations:

$$(\mathbf{D}_{LM}\mathbf{H}^\dagger D\mathbf{H}\mathbf{D}_{LM} + \sigma\mathbf{D}_{LM})\mathbf{b}_2 = \mathbf{D}_{LM}\mathbf{f}^*, \tag{34}$$

from which the solution at the time instant t_k is obtained as $q_m(t_k) = -2b_{2,(m-1)L}$.

The last equation is the analog of that derived in [38] for the scalar GLME (i.e., when $M = 1$), where it is numerically solved using the conjugate gradient method by taking advantage of the fact that the system's matrix is symmetric and positive-defined, and of the Hankel shape of the matrices involved. Unfortunately, while the conjugate gradient method can also be used in our case, the matrix $\mathbf{H}$ in Eq. (34) is not Hankel, and therefore, the matrix multiplication may be a computationally demanding task for our problem. However, Eq. (34) is equivalent to the following system of equations:

$$A_{m,1}\mathbf{b}_{2,1} + \cdots + A_{m,M}\mathbf{b}_{2,M} + \sigma D\mathbf{b}_{2,m} = D\mathbf{f}_m^*, \tag{35}$$

Optics EXPRESS

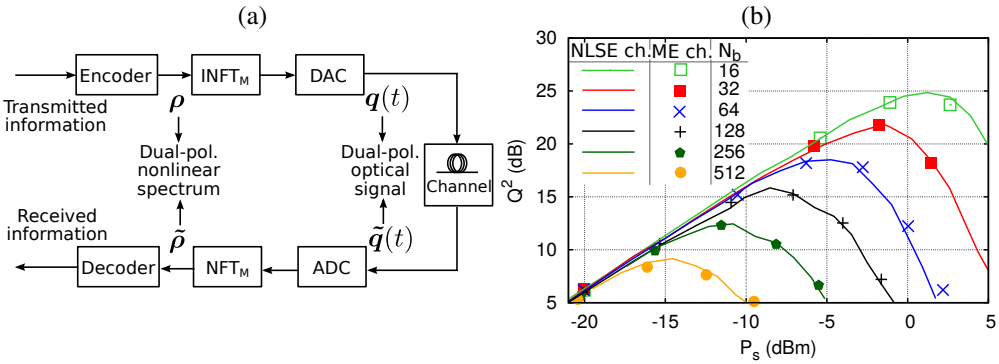

Fig. 2. (a) Basic PDM-NIS scheme; (b) Performance (Q^2-factor) of single polarization modulation over the ME channel model (symbols only), where both polarization components are corrupted by noise, compared to that over the NLSE channel model (solid lines) (similar to systems considered in Refs. [18, 32]).

for $m = 1, \ldots, M$, where $A_{m,n} = DH_m^\dagger DH_n D$, and H_m-s are the Hankel matrices. Consequently, system (34) can now be solved with the conjugate gradient method through Eq. (35), starting with an initial guess for $\mathbf{b}_2$ (e.g., the null vector) and iteratively updating the solution, and performing the products involved with help of FFTs as explained at the beginning of this subsection.

The method explained above should be independently applied to find the solution in any time instant t_k of interest. However, if the solution has to be found in the whole interval $[-T, T]$, several iterations can be saved starting from $t_{N_t+1} = T$, and later for t_k considering as a starting point for $\mathbf{b}_2$ the vector found in the previous step, at the adjacent time instant t_{k+1}.

In this work, we considered the nonlinear spectrum *from the right* defined as $\boldsymbol{\rho}(\lambda) = \mathbf{b}(\lambda)/a(\lambda)$ [4] (i.e. the right reflection coefficient), and the corresponding VGLME given by Eq. (5). However, one can also consider the nonlinear spectrum *from the left* $\boldsymbol{\rho}_l(\lambda) = \mathbf{b}(\lambda)^*/a(\lambda)$ [4] and its corresponding VGLME, which is different from Eq. (5) but can be obtained from it [38]. The authors of [38], considering the scalar NLSE case only, claim that while from a theoretical point of view we can equivalently use one nonlinear spectrum (left or right) instead of the other, from the numerical point of view, the accuracy of the numerical method can be significantly improved by considering the standard GLME from the right to find the time domain signal in time instants $t_k \geq 0$, and the GLME from the left for $t_k < 0$. We expect that the same should hold for the VGLME, however, in this work, we used only the standard VGLME (5).

A full optimization of the method that takes into account also the nonlinear spectrum from the left, as well as investigations about the accuracy of the method and its stability will be the subject of a future work.

4. System setup and simulation results

The system setup is sketched in Fig. 2(a), and is the natural dual-polarization extension of the NIS scheme considered in [39]. At the TX, information is mapped on two quadrature phase-shift keying (QPSK) signals $s_i(t)$, $i = 1, 2$, with a shaping pulse having a root-raised cosine FT with roll-off $\beta = 0.2$, and symbol rate $R_s = 50\,\text{GBd}$. The FT of each $s_i(t)$, $S_i(f)$, is mapped to the nonlinear spectrum (3) according to $\rho_i(\lambda) = -S_i(-\lambda/\pi)$, for $i = 1, 2$. The dual polarization optical signal $\mathbf{q}(t)$ is obtained performing an INFT$_\text{M}$ of the dual polarization nonlinear spectrum $\boldsymbol{\rho}(t) = (\rho_1(\lambda), \rho_2(\lambda))$. Next, the analog signal is obtained with a digital-to-analog converter (DAC) and sent into the channel. The channel is a SSMF (GVD parameter $\beta_2 = -20.39\,\text{ps}^2/\text{km}$, nonlinear coefficient $\gamma = 1.22\,\text{W}^{-1}\text{km}^{-1}$, and attenuation $\alpha_\text{dB} = 0.2\,\text{dB/km}$) of length $L = 2000\,\text{km}$ with ideal distributed amplification having spontaneous emission factor $\eta_{sp} = 4$. A preliminary study

Optics EXPRESS

about the impact of PMD on the NFT-based transmission showed that it can be compensated with a very small performance degradation [21], such that we neglect the impact of PMD in the current work. At the end of the channel, the analog-to-digital converter (ADC) recovers the samples of received signals, from which the received nonlinear spectrum is retrieved through the NFT_M block. A noise-corrupted version of $\rho_i(\lambda)$, $i = 1, 2$, is obtained from the received signal and multiplied by $e^{4j\lambda^2\mathcal{L}}$ to remove the deterministic propagation effects, with $\mathcal{L}$ being the normalized channel length (we also do not pre-compensate the dispersive spreading at the TX side). Finally, matched filtering and sampling are used to recover the transmitted information symbols. Both the DAC and ADC have bandwidth $B = 100\,\text{GHz}$. It is important to remark that, while the operations concerning symbol mapping (detection) on (from) the nonlinear spectrum are performed independently on the two polarizations, NFT_M and INFT_M are performed jointly (and the result depends on both polarizations) to ensure the integrability of the channel (1). As customary when using the NFT with vanishing boundary conditions, the transmission is organized in bursts [32, 39], each carrying N_b information symbols per polarization, and separated by N_z guard symbols that do not carry any information to avoid inter-burst interference. In this work, $N_z = 800$ is considered to account for the overall memory due to linear dispersion, which is of the order of $2\pi L|\beta_2|R_s^2(1+\beta) \sim 768$ symbols, as in [39].

Simulation performance is measured in terms of Q-factor as $Q^2_{\text{dB}} = 20\log_{10}[(\sqrt{2}\text{erfc}^{-1}(2\text{BER})]$, where bit error rate (BER) is estimated through the error vector magnitude [40]. The average power per symbol, P_s, is defined as $P_s = E_s R_s$, where R_s is the symbol rate and E_s is the average energy per information symbol,

$$E_s = \begin{cases} (2N_b)^{-1}\int_{-\infty}^{+\infty}\left(|Q_1(T)|^2 + |Q_2(T)|^2\right)dT & \text{dual pol.} \\ \\ (N_b)^{-1}\int_{-\infty}^{+\infty}\left(|Q_1(T)|^2\right)dT & \text{single pol.} \end{cases}. \tag{36}$$

The NFT_M and INFT_M operations are implemented by using the numerical methods presented in Section 3, considering the case $M = 2$ for the ME. Unless otherwise stated, an oversampling factor of 4 samples per symbols is used; higher oversampling factors are considered in Figs. 3(b) and 5(b).

Most of the works dealing with the NFT-based transmission schemes consider the NLSE (single-polarization) channel model. However, in practical transmission systems, in-line amplifiers generate noise on both polarizations, thus making $q_2(t)$ always non null. Therefore, the two polarizations can interact with each other due to the nonlinear coupling term present in the ME. To investigate the possible impact of this coupling, Fig. 2(b) compares the performance obtained with the single-polarization NIS scheme assuming the NLSE as a channel model, with that obtained with single-polarization modulation but assuming the full ME as a channel model, i.e. by modulating just one polarization of the ME, letting the other grow during propagation due to in-line noise, and eventually discarding it at the RX. The figure shows that the systems performance does not change noticeably, meaning that the noise in the second polarization does not affect the NIS performance. Note that it might not be the case for other parameter ranges, transmission schemes, or detection strategies.

In Fig. 3(a) we show with solid lines the PDM-NIS performance as a function of the optical power for different burst lengths N_b. For the sake of comparison, the dashed lines in the same figure show the results obtained in the same system when we modulate only one polarization and set the other one to zero. We remark that, while the same colors correspond to the same burst lengths N_b, the number of information symbols is doubled when considering the PDM-NIS compared to the single-polarization NIS. The figure shows that the PDM-NIS performance is slightly worse than that obtained for single-polarization NIS. This difference increases up to about 1 dB for longer bursts. We conjecture that this degradation is due to the doubled energy of

Optics EXPRESS

the received signal, which might affect the strength of the perturbation caused by noise on the nonlinear spectrum. Indeed, some theoretical studies [14, 41] indicate that, when considering the NLSE model, the intensity of the noise affecting the nonlinear spectrum increases with the spectrum itself. However, to the best of our knowledge, similar studies are not available for the ME.

Importantly, the decay of PDM-NIS (and NIS) performance with the burst length is caused by noise and not by numerical inaccuracies, as demonstrated in the following. In fact, Figure 3(b) compares the performance of PDM-NIS in a noisy and ideal noise-free (n.f.) scenario, and with actual and increased numerical accuracy for the INFT and NFT computation. The decay of the n.f. performance at higher power is a typical behavior of NFT-based schemes, and is due to the fact that, at higher powers, the system is more sensitive to numerical inaccuracies. Consequently, a higher numerical accuracy provides a better performance in the n.f. scenario. On the other hand, in the noisy scenario, the impact of noise is much stronger than that of numerical inaccuracy (as testified by the significant performance decrease compared to the n.f. scenario), such that PDM-NIS achieves the same performance with standard or increased numerical accuracy. Similar conclusions were drawn for single-polarization NIS systems [39].

Furthermore, we investigated the different impact of numerical errors in the NFT and INFT operations. In particular, we considered the samples of the nonlinear spectrum $\boldsymbol{\rho}(\lambda)$ obtained for PDM-NIS (same scenario considered in Figs. 3(a) and 3(b) with $N_b = 32$), and we applied one INFT and one NFT to obtain the samples of $\tilde{\boldsymbol{\rho}}(\lambda) = \mathrm{NFT}(\mathrm{INFT}(\boldsymbol{\rho}(\lambda))$. Fig. 4(a) shows the normalized mean square error (NMSE) on the nonlinear spectrum defined as

$$\mathrm{NMSE} = \left(\sum_{m=1,2} \sum_{k=1}^{N_{\mathrm{sa}}} |\rho_{k,m} - \tilde{\rho}_{k,m}|^2 \right) \left(\sum_{m=1,2} \sum_{k=1}^{N_{\mathrm{sa}}} |\rho_{k,m}|^2 \right)^{-1} \tag{37}$$

where N_{sa} is the number of samples for the nonlinear frequencies λ, and $\rho_{k,m}$ and $\tilde{\rho}_{k,m}$ are the k-th samples of $\rho_m(\lambda)$ and $\tilde{\rho}_m(\lambda)$, respectively. The figure shows the NMSE for different oversampling factors for the NFT and the INFT—denoted as N_D and N_I, respectively. The blue curve ($N_D = N_I = 4$) represents the error obtained with the oversampling factor actually employed in most of the simulations shown in this work, while the red one ($N_D = N_I = 16$) can be taken as a high-accuracy "reference"; the different impact on error of the two NFT operations is shown by decreasing N_D and N_I, one at a time, from 16 to 4. It turns out that, for the considered overampling factor of 4, numerical errors are mostly due to the NFT in the higher power region, and to the INFT in the lower power region.

5. Reduced complexity system

The ME (2) describes the propagation of a normalized dual-polarization optical signal in the fiber channel, accounting for the interaction between the two polarizations induced by the nonlinear term. Accordingly, the PDM-NIS encodes and decodes information on the nonlinear spectrum using the $\mathrm{NFT_M}$ associated with the ME, as in Fig. 2(a), avoiding nonlinear interference. The ME does not entail any exchange of energy between the two signal polarisations, which suggests that modeling their propagation by two independent NLSEs might provide a reasonable approximation. In this case, the NIS transmission scheme could be implemented independently on each polarization according to the $\mathrm{PDM\text{-}NIS_{NLS}}$ scheme shown in Fig. 4(b). This approximated approach neglects the interaction between the two polarizations during propagation, giving rise to some nonlinear interference. At the same time, using two $\mathrm{NFT_{NLS}}$ instead of a single $\mathrm{NFT_M}$ reduces the overall processing complexity, as will be clear later in this section. It is therefore interesting to see what is the impact of the introduced simplification on the performance of the NIS system.

To address this problem, we compare the achievable performance of PDM-NIS with

Optics EXPRESS

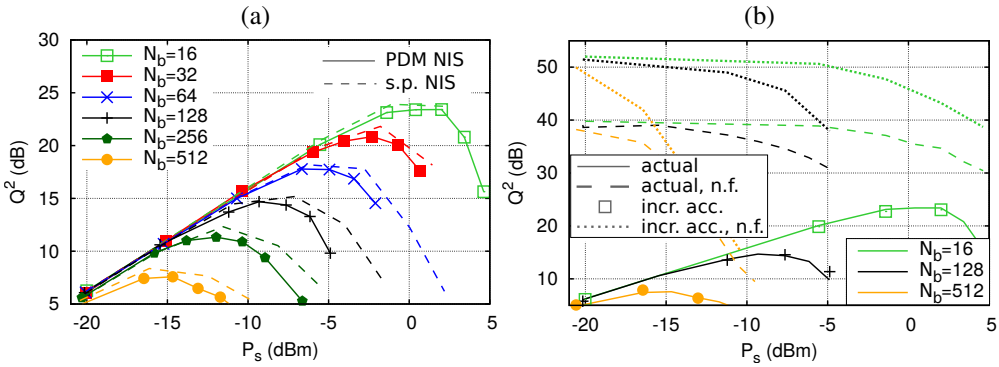

Fig. 3. Performance for different burst lengths with same color: (a) PDM-NIS performance compared with single polarization NIS; and (b) PDM-NIS in the noisy and noise-free scenarios, with actual (4 samples per symbol) and increased (8 samples per symbol) accuracy for NFTs.

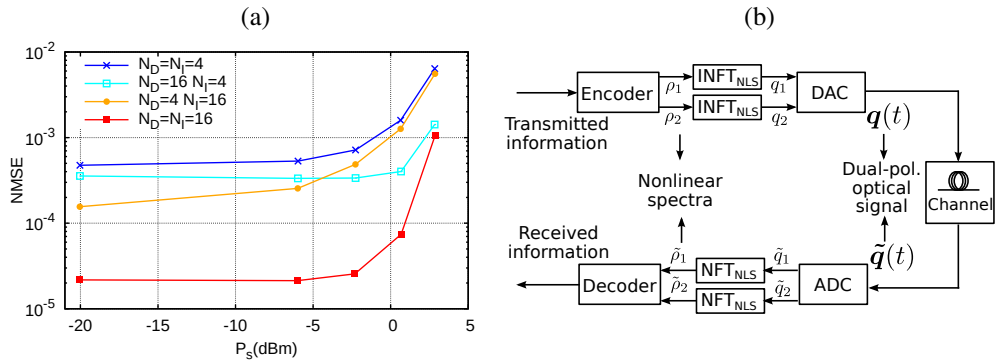

Fig. 4. (a) NMSE on the nonlinear spectrum after INFT and NFT as a function of the optical power, for different oversampling factors; (b) PDM-NIS_{NLS} scheme.

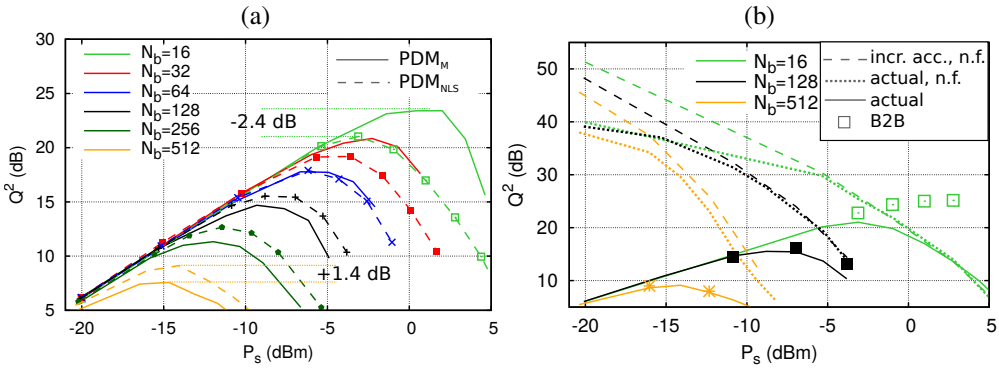

Fig. 5. Performance Vs power per symbol for different burst lengths with same color: (a) PDM-NIS (solid lines) compared with reduced complexity PDM-NIS_{NLS} (dashed lines); (b) PDM-NIS_{NLS} compared with PDM-NIS_{NLS} n.f. with actual (4 samples per symbol) and increased (8 samples per symbol) accuracy, and with back-to-back performance.

Optics EXPRESS

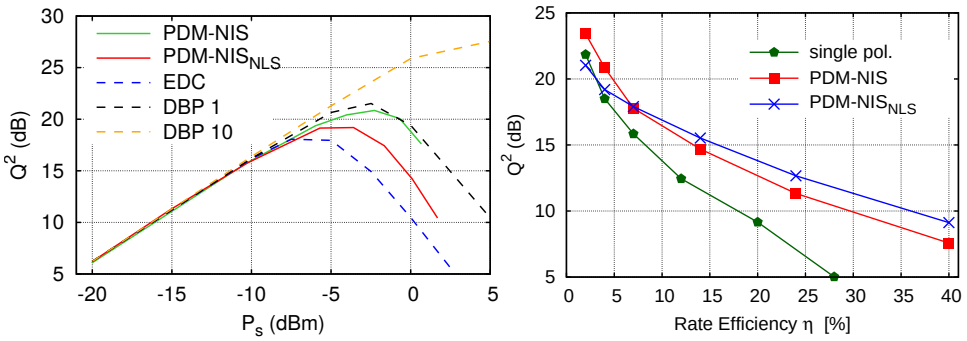

Fig. 6. (a) Performance Vs power per symbol for $N_b = 32$ for PDM-NIS, PDM-NIS$_{NLS}$, and conventional systems; (b) Optimal performance as a function of the rate efficiency.

PDM-NIS$_{NLS}$ depicted, respectively, in Figs. 2(a) and 4(b). Simulation results are shown in Fig. 5(a) for different burst lengths. At lower powers, the performance of PDM-NIS$_{NLS}$ and PDM-NIS is the same. Indeed, in the linear regime, the nonlinear term in the ME (2), which accounts for polarization mixing, tends to zero. Consequently, the two transmission schemes are equivalent. At higher powers, the two schemes perform differently. For shorter bursts (e.g., $N_b = 16, 32$) PDM-NIS$_{NLS}$ performs worse, as expected, due to the mismatch between the transmission scheme (designed for the NLSE) and the actual channel (modelled by the ME). On the other hand, increasing the burst length, the performance difference decreases and, for long burst (e.g., $N_b = 256, 512$), PDM-NIS$_{NLS}$ performs even slightly better than PDM-NIS. We conjecture that this unexpected behavior has the same physical origin as the performance degradation of PDM-NIS compared to single-polarization NIS observed in Fig. 3(a). Indeed, in PDM-NIS$_{NLS}$, detection is made by separately considering the NFT$_{NLS}$ spectrum of each polarization, whose energy is only one half that of the total signal. Therefore, recalling that the intensity of the perturbation of the nonlinear spectrum caused by noise depends on the signal energy, we expect the NFT$_{NLS}$ spectrum of each polarization to be less affected by noise than the NFT$_M$ spectrum of the whole signal. This effect is more evident for higher signal energies, i.e., for longer bursts, when it becomes stronger than the mismatch between the transmission scheme and the channel. This outcome shows that, in the region where this effect is evident, signal noise interaction in the joint processing strongly affects performance hiding the benefit of considering ME to include polarization interaction. Finally, it is worth noting that for longer bursts, PDM-NIS$_{NLS}$ performs similarly to the single polarization NIS, cf. Fig. 3(a).

Figure 5(b), which shows the performance of PDM-NIS$_{NLS}$ (i) with dotted line, (ii) in the ideal n.f. scenario with solid line, (iii) in the ideal n.f. scenario and with increased accuracy for the NFTs with dashed lines, and (iv) in the back-to-back configuration with symbols only, supports our conjecture, as explained in the following. Firstly, Fig. 5(b) shows that at higher powers the PDM-NIS$_{NLS}$ performance coincides with the n.f. performance, indicating that the performance decay does not originate from noise. Secondly, the performance of PDM-NIS n.f., which is shown in Fig. 3(b), equals that of PDM-NIS$_{NLS}$ at lower powers, but PDM-NIS performs better at higher powers, indicating that the system does not account for the polarization mixing occurring at high powers. Thirdly, when increasing accuracy, the performance of PDM-NIS$_{NLS}$ n.f. increases at lower powers, where the polarization mixing is negligible, but does not improve at higher powers. Moreover, the performance improves for $N_b = 16, 128$ in the back-to-back configuration, i.e, without channel, but with an equivalent noise. The latter two facts confirm that the performance degradation occurs due to the polarizations' interaction.

Another transmission scheme that can be considered (i) modulates the information according

Optics EXPRESS

to the NFT_M, i.e., in agreement with the channel model, and (ii) retrieves the information using two NFT_NLS. This scheme inserts a discrepancy at the receiver (RX), but might reduces the noise on the nonlinear spectrum, following the reasoning considered above. However, while in PDM-NIS_NLS TX and RX agree with each others and errors occur because of the presence of the channel, the last scheme also introduces a discrepancy in back-to-back configuration. As a consequence, this transmission scheme, that does not provide a significant complexity reduction, is not comparable with PDM-NIS_NLS in terms of performance.

Figure 6(a) compares for $N_b = 32$ the performance of PDM-NIS and PDM-NIS_NLS with those of electronic dispersion compensation (EDC) and digital backpropagation (DBP) with 1 and 10 step per span. The figure shows that PDM-NIS and PDM-NIS_NLS both outperform EDC, while DBP with 1 step per span is comparable with PDM-NIS; DBP with 10 step per span outperforms the other schemes. This result is in accordance with that obtained for single polarization in [39], and we expect to obtain the same behavior shown in [39] for different values of N_b. Also, a comparison with conventional systems for dual polarization systems has been shown in [21], which reports results more favorable for NFT based schemes. However, we mention that the NFDM schemes are expected to provide the best improvements with respect to conventional systems when the multi-channel transmission in the network scenario with ROADMs is considered, while this manuscript considers a single channel (a point-to-point transmission). Also, while the final goal of NFDM systems is to outperform conventional systems, overcoming the limitations imposed by nonlinearity, this work aims to investigate about dual polarization NIS schemes, to provide a tool that, once optimized, might compete with conventional systems. An interested reader can find more comparisons between PDM NFT-based systems and OFDM in [21] and comparisons in single polarization in [16, 32, 39].

Figure 6(b) compares the performance of three schemes introduced—namely, single-polarization NIS, PDM-NIS, and PDM-NIS_NLS—as a function of the rate efficiency, which accounts for the loss in spectral efficiency due to the insertion of guard times, and the overall number of information symbols sent [39]. The rate efficiency η is defined as the ratio between the number of information symbols and the total number of symbols,

$$\eta = \begin{cases} N_b/2(N_z + N_b) & \text{single polarization,} \\ N_b/(N_z + N_b) & \text{dual polarization.} \end{cases} . \tag{38}$$

Firstly, Fig. 6(b) shows that, thanks to the use of both polarizations, PDM-NIS performs better than single-polarization NIS, doubling the rate efficiency with only a small performance degradation. Secondly, for a low rate efficiency, PDM-NIS_NLS performs worse than both dual and single-polarization NIS, as a result of neglecting polarizations' interaction. On the other hand, at a higher rate efficiency, PDM-NIS_NLS performs slightly better (around 1 dB) even than PDM-NIS, thanks to the lower impact of noise on the NFT_NLS spectrum. In this work precompensation is not deployed, but can be used to halve the number of guard symbols N_z and, thus, increase the spectral efficiency [42, 43]. This, however, would not change the overall behavior of Fig. 6.

We note that, while the NFT_M theory required for double-polarization NFT-based communication systems can be deemed a straightforward extension of the NFT_NLS theory, it can bring about some difficulties in terms of developing fast and accurate numerical algorithms for NFT_M computation, in particular taking into account that the research for fast numerical NFT_NLS is still in progress (see [4] and references therein). Indeed, the computational complexity depends on the algorithms deployed and further work is required in this direction. However, we expect the computational complexity of PDM-NIS_NLS to be typically lower than that of PDM-NIS because of an extra dimension entering the operations involved in the latter. These aspects might become even more relevant when increasing the number of dimensions, e.g., by extending the PDM-NIS concept and the complexity reduction approach based on PDM-NIS_NLS to SDM systems in multicore or multimode fibers. Indeed, considering the general case with $M \geq 2$, the RX should

Optics EXPRESS

solve M 2×2 or one $(M+1) \times (M+1)$ Zakharov-Shabat eigenvalue problem; let $C(M, N_{\mathrm{sa}})$ denote its computational cost, $N_{\mathrm{sa}} \geq 1$ being the number of samples for the time axis. With this notation the reduced complexity RX would be less computationally complex if and only if

$$MC(1, N_{\mathrm{sa}}) < C(M, N_{\mathrm{sa}}). \tag{39}$$

This equation is true for the algorithm presented in Subsection 3.1 since, in this case, $C(M, N_{\mathrm{sa}}) = N_{\mathrm{sa}}(M+1)^2$. Moreover, we expect Eq. (39) to hold also with faster algorithms as the discretized time domain signal has $N_{\mathrm{sa}}M$ samples and a sufficient condition for Eq. (39) to hold is that $C(M, N_{\mathrm{sa}})$ depends more than linearly on M.

However, we recall that the reduced-complexity system performs better only in some specific scenarios (when the perturbation of the nonlinear spectrum due to noise dominates the performance) and for the considered detection strategy. In fact, we expect that when dealing with improved detection strategies which can avoid the aforementioned detrimental perturbation of the nonlinear spectrum [44, 45], a joint processing of all the system modes (polarizations) by the $\mathrm{NFT_M}$ might be required to obtain the optimal performance.

As an end note, we would like to remark an important difference between PDM-NIS and PDM-$\mathrm{NIS_{NLS}}$, which regards the (slowly varying in time) polarization rotation induced on a signal during propagation, which can be modeled as a multiplication by a unitary matrix R. As far as it concerns the first scheme, this rotation can be removed both in time (i.e., before the NFT) or in the nonlinear frequency domain (i.e., after the NFT), multiplying for $R^{-1} = R^{\dagger}$ or $R^{*-1} = R^{T}$, respectively, as a consequence of Eq. (12). The latter solution allows to directly employ the same digital processing techniques that are used in conventional systems to this end. On the other hand, the same can not be done for PDM-$\mathrm{NIS_{NLS}}$ since a property similar to Eq. (12) does not hold. Indeed,

$$\begin{bmatrix} \mathrm{NFT_{NLS}}\left(R_{11}q_1 + R_{12}q_2\right) \\ \mathrm{NFT_{NLS}}\left(R_{21}q_1 + R_{22}q_2\right) \end{bmatrix} \neq \begin{bmatrix} R_{11}^{*}\mathrm{NFT_{NLS}}\left(q_1\right) + R_{12}^{*}\mathrm{NFT_{NLS}}\left(q_2\right) \\ R_{21}^{*}\mathrm{NFT_{NLS}}\left(q_1\right) + R_{22}^{*}\mathrm{NFT_{NLS}}\left(q_2\right) \end{bmatrix}, \tag{40}$$

since the NFT is not a linear operation and $|R_{n,m}| \neq 1$ for $n, m = 1, 2$ (moreover, one can easily show numerical counterexamples, e.g., considering $R_{11} = R_{12} = R_{22} = 1/\sqrt{2}$ and $R_{21} = -1/\sqrt{2}$). The lack of a similar property implies that the polarization rotation in PDM-$\mathrm{NIS_{NLS}}$ should be removed in time domain, before the NFT, which might require a non straightforward extension of the digital signal processing techniques commonly employed in conventional systems.

6. Conclusion

This work dealt with the dual polarization NFT-based transmission schemes, exploiting NLSE and ME integrability. After a brief review regarding the validity of this two equations as models for the propagation in SSMF, we presented two numerical methods for the computation of the NFT operations for the general M-dimensional VNLSE, which apply to both NLSE and ME. Next, we introduced a polarization and nonlinear frequency-division scheme—PDM-NIS—that, following its analogy with the NLSE-based NIS for one polarization, encodes the information on the continuous nonlinear spectrum. We showed that the PDM-NIS achieves almost the same performance as we have for one-component NIS but doubling the number of information symbols transmitted. Moreover, we introduced the reduced-complexity PDM-$\mathrm{NIS_{NLS}}$ transmission scheme that, similarly to PDM-NIS, encodes and decodes information on the nonlinear spectrum, but using two scalar $\mathrm{NFT_{NLS}}$ rather than one $\mathrm{NFT_M}$. This scheme, which neglects polarization mixing occurring during the propagation, provides a complexity reduction, not only from a computational point of view (a lower number of floating point operations required), but also allow us to avoid the possible difficulties arising in the $\mathrm{NFT_M}$ theory and algorithms. Remarkably, despite the mismatch with the channel model, the performance of PDM-$\mathrm{NIS_{NLS}}$ is not only comparable with

Optics EXPRESS

PDM-NIS at some parameters range, but can also provides a slight performance improvement at sufficiently high rate efficiency.

As a future work, it is important to understand the impact of adding discrete spectral components modulation to the schemes presented here. Also, it might be interesting to understand whether the reduced complexity scheme can be used with other detection strategies [44, 45], or within SDM-NIS schemes, having in mind that the complexity of NFT operations associated with VNLSE further increases. Finally, for the PNFDM schemes to be fully competitive with other nonlinearity mitigation techniques, it is important to develop fast numerical algorithms for both the direct and inverse NFT operations for ME.

Funding

Erasmus + mobility programme; EPSRC Programme (TRANSNET); Leverhulme Project (RPG-2018-063); POR FESR (FIPILI3).